Report

Current Biology

Hec1 Tail Phosphorylation Differentially Regulates Mammalian Kinetochore Coupling to Polymerizing and Depolymerizing Microtubules

Graphical Abstract

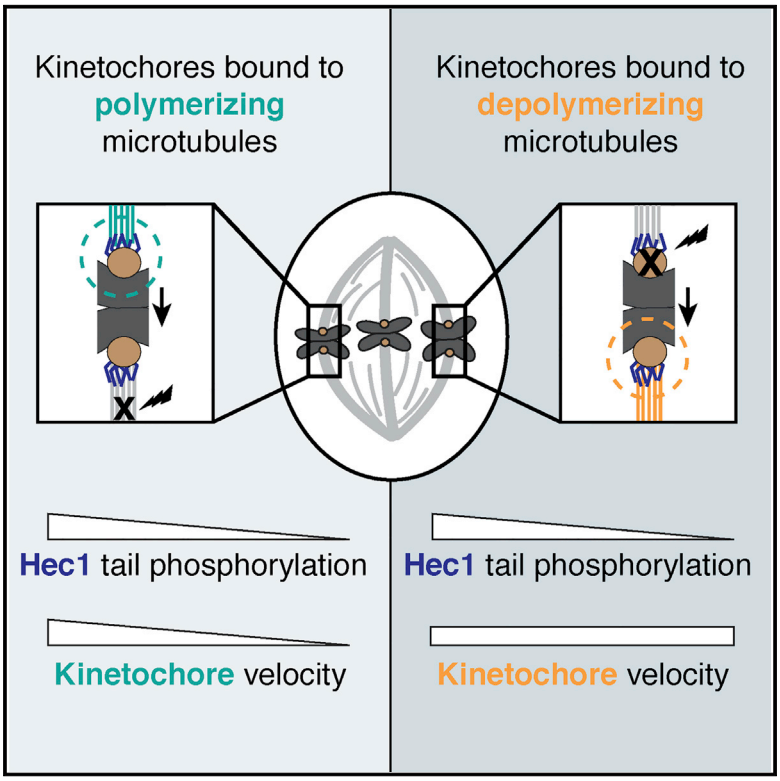

Authors

Alexandra F. Long, Dylan B. Udy, Sophie Dumont

Correspondence

sophie.dumont@ucsf.edu

In Brief

Kinetochores link chromosomes to dynamic spindle microtubules. Long et al. demonstrate that phosphorylation of Hec1, a key component of kinetochore-microtubule attachments, tunes resistive friction on polymerizing microtubules without jeopardizing the active force generation by depolymerizing microtubules that powers chromosome movement.

Highlights

- Laser ablation can isolate kinetochores in different polymerization states in vivo
- Hec1 tail phosphorylation regulates kinetochore velocity on growing microtubules
- Hec1 tail phosphorylation does not disrupt coupling to shrinking microtubules
- Hec1 regulation differentially affects coupling to growing versus shrinking microtubules

Long et al., 2017, Current Biology *27*, 1–8
June 5, 2017
http://dx.doi.org/10.1016/j.cub.2017.04.058

CellPress

Please cite this article in press as: Long et al., Hec1 Tail Phosphorylation Differentially Regulates Mammalian Kinetochore Coupling to Polymerizing and Depolymerizing Microtubules, Current Biology (2017), http://dx.doi.org/10.1016/j.cub.2017.04.058

Current Biology
Report

Hec1 Tail Phosphorylation Differentially Regulates Mammalian Kinetochore Coupling to Polymerizing and Depolymerizing Microtubules

Alexandra F. Long,[1,2] Dylan B. Udy,[2,3] and Sophie Dumont[1,2,4,5,*]
[1]Tetrad Graduate Program
[2]Department of Cell and Tissue Biology
University of California, San Francisco, San Francisco, CA 94143, USA
[3]MCB Graduate Program, University of Washington, Seattle, WA 98195, USA
[4]Department of Cell and Molecular Pharmacology, University of California, San Francisco, San Francisco, CA 94143, USA
[5]Lead Contact
*Correspondence: sophie.dumont@ucsf.edu
http://dx.doi.org/10.1016/j.cub.2017.04.058

SUMMARY

The kinetochore links chromosomes to dynamic spindle microtubules and drives both chromosome congression and segregation. To do so, the kinetochore must hold on to depolymerizing and polymerizing microtubules. At metaphase, one sister kinetochore couples to depolymerizing microtubules, pulling its sister along polymerizing microtubules [1, 2]. Distinct kinetochore-microtubule interfaces mediate these behaviors: active interfaces transduce microtubule depolymerization into mechanical work, and passive interfaces generate friction as the kinetochore moves along microtubules [3, 4]. Despite a growing understanding of the molecular components that mediate kinetochore binding [5–7], we do not know how kinetochores physically interact with polymerizing versus depolymerizing microtubule bundles, and whether they use the same mechanisms and regulation to do so. To address this question, we focus on the mechanical role of the essential load-bearing protein Hec1 [8–11] in mammalian cells. Hec1's affinity for microtubules is regulated by Aurora B phosphorylation on its N-terminal tail [12–15], but its role at the interface with polymerizing versus depolymerizing microtubules remains unclear. Here we use laser ablation to trigger cellular pulling on mutant kinetochores and decouple sisters in vivo, and thereby separately probe Hec1's role on polymerizing versus depolymerizing microtubules. We show that Hec1 tail phosphorylation tunes friction along polymerizing microtubules and yet does not compromise the kinetochore's ability to grip depolymerizing microtubules. Together, the data suggest that kinetochore regulation has differential effects on engagement with growing and shrinking microtubules. Through this mechanism, the kinetochore can modulate its grip on microtubules over mitosis and yet retain its ability to couple to microtubules powering chromosome movement.

RESULTS

Targeted Control of Cellular Pulling Forces on Kinetochores In Vivo

To probe Hec1's mechanical role at the mammalian kinetochore-microtubule interface, we sought the ability to exert force on a given kinetochore inside a cell at a specific time. This is necessary to probe the magnitude and timescale of a kinetochore's response to force, and to perturb kinetochores moving on microtubules in a given polymerization state. We accomplished this using targeted laser ablation to sever one kinetochore-fiber (k-fiber) at metaphase (Figure 1A). The newly created k-fiber minus ends recruit dynein, which in turn exerts a poleward pulling force on the attached kinetochore and its sister [16, 17].

As a starting point for our Hec1 studies, we expressed Hec1-EGFP in PtK2 cells depleted of endogenous Hec1 by RNAi [11]. We selectively severed polymerizing k-fibers near their kinetochore, and examined the responses of both the "front" and "back" sister kinetochores (proximal and distal to the cut, respectively) (Figures 1A and 1B; Movie S1). The response to laser ablation appeared the same as in wild-type cells [16, 17], and had two phases (Figures 1B and 1E–1G, blue traces; Table 1; n = 13). First, the front kinetochore recoiled immediately after being cut, reflecting a decrease in force and causing the inter-kinetochore (K-K) distance to decrease. Second, dynein pulled the microtubules bound to the front kinetochore, moving the sister pair toward the ablation site and increasing the K-K distance. Dynein pulled the front sister faster than its k-fiber polymerized or depolymerized, and faster than normal metaphase movements [16] (Table 1). The front kinetochore's velocity during dynein-mediated movement was similar between experiments (Figures 1F and 1H, blue traces; Table 1), consistent with ablation triggering a consistent response. Dynein pulling caused the back kinetochore to turn around within seconds, ultimately pulling it away from its pole along polymerizing microtubules. Thus, targeted k-fiber ablation can produce a pulling force to probe the mechanics of the interface between kinetochores and polymerizing microtubules.

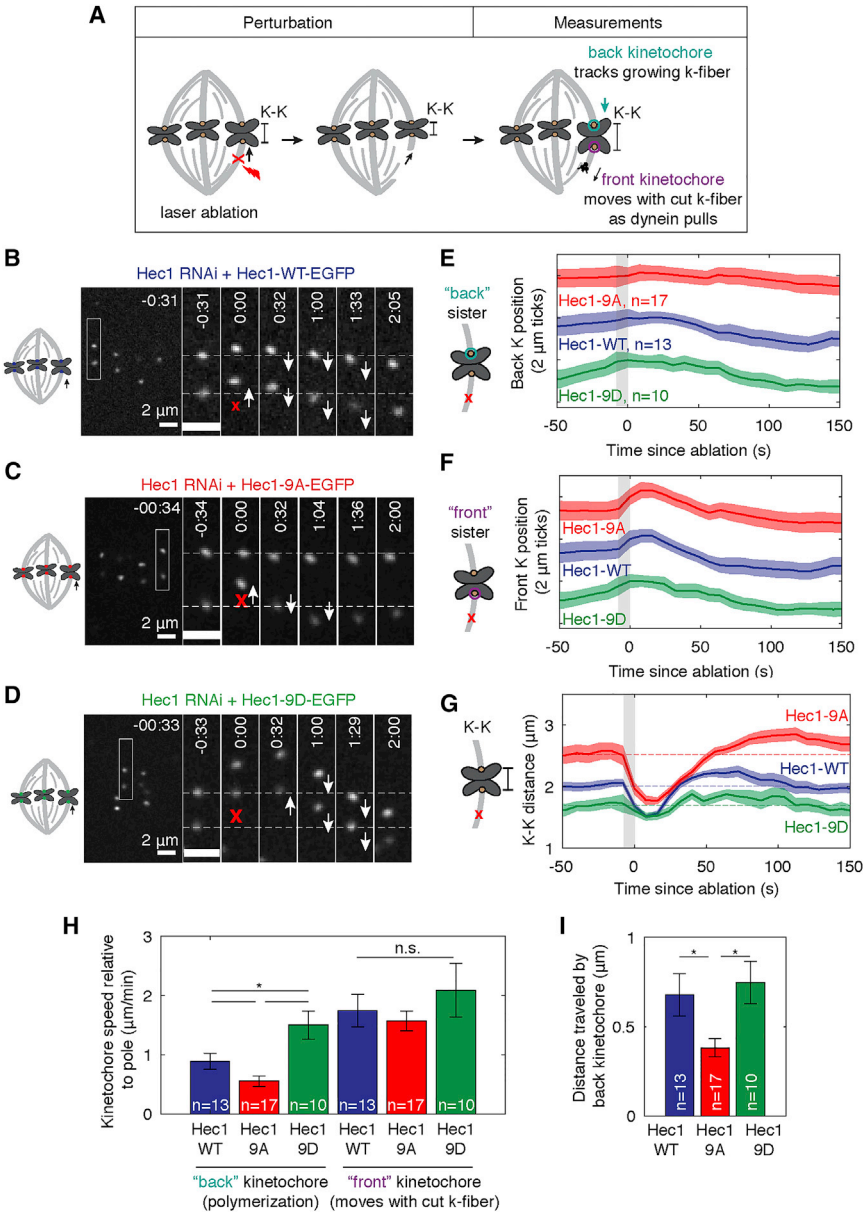

Figure 1. Hec1 Tail Phosphorylation Regulates the Magnitude and Timescale of the Mammalian Kinetochore-Microtubule Interface's Response to Force

(A) Assay to sever a k-fiber using laser ablation (red X) to induce a dynein-based poleward pulling force on a specific kinetochore pair to probe the back kinetochore's movement on polymerizing microtubules in response to force.

(B–D) Time lapse showing representative responses of PtK2 (B) Hec1-WT-EGFP, (C) Hec1-9A-EGFP, and (D) Hec1-9D-EGFP (each in Hec1 RNAi background; see also Figure S1) kinetochore pairs to k-fiber laser ablation. First frame after ablation is set to 0:00.

(E–G) Mean positions of Hec1-WT, Hec1-9A, and Hec1-9D (E) back and (F) front kinetochores and (G) K-K distance before and after laser ablation. Kinetochore position is shown normalized to its pre-ablation position. Traces are mean ± SEM and are offset vertically for clarity in (E) and (F).

(H) Velocity of the front and back kinetochores (from E and F) relative to the ablation-proximal spindle pole after the directional switch to poleward motion in response to ablation, until each kinetochore returned to motion away from that pole (error bars, mean ± SEM; *$p < 0.05$, Student's t test; n.s., not significant; n, number of kinetochores).

(I) Distance traveled by the back kinetochore over the first 30 s of poleward motion after ablation (error bars, mean ± SEM; *$p < 0.05$, Student's t test).

See also Figure S1 and Movies S1, S2, and S3.

Hec1 Tail Phosphorylation Regulates the Magnitude and Timescale of the Mammalian Kinetochore-Microtubule Interface's Response to Force

To probe the mechanical regulation conferred by Hec1's N-terminal tail phosphorylation during mitosis, we asked whether and how it controls the movement of a kinetochore in response to force. We depleted endogenous Hec1 by RNAi (Figure S1) and expressed either Hec1-9A-EGFP or Hec1-9D-EGFP to mimic constitutive dephosphorylation and phosphorylation, respectively, a range that includes typical Hec1 phosphorylation by Aurora B during mitosis [14]. Expression levels of Hec1-WT-EGFP, Hec1-9A-EGFP, and Hec1-9D-EGFP were indistinguishable (Figure S1). As expected [14], Hec1-9D and Hec1-9A kinetochores resulted in different steady-state K-K distances (Figures 1C, 1D, and 1G; Table 1).

We subjected these Hec1-9A (Figures 1E–1G, red traces; n = 17; Movie S2) and Hec1-9D kinetochores (Figures 1E–1G, green traces; n = 10; Movie S3) to the same force signature as Hec1-WT, as suggested by similar front kinetochore velocities during dynein pulling (Figure 1H; Table 1). As with Hec1-WT, after k-fiber ablation, the front kinetochore recoiled and the K-K distance decreased in both Hec1-9A and Hec1-9D cells. When dynein pulling engaged, however, the back sister responses were different from Hec1-WT. In Hec1-9A cells, the back kinetochore moved more slowly than its front sister (0.6 ± 0.1 versus 1.6 ± 0.2 μm/min; Table 1), and moved less far than Hec1-WT (0.4 ± 0.1 versus 0.7 ± 0.1 μm; Figures 1H and 1I; Table 1). These differences led to a larger, and longer-lasting, increase in K-K distance above baseline during dynein pulling compared to Hec1-WT (maximum K-K distance was at 95 ± 7 versus 47 ± 5 s; Figure 1G; Table 1). In contrast, in Hec1-9D cells, the back sister followed at a rate similar to its front sister (1.7 ± 0.4 versus 1.8 ± 0.2 μm/min), which is faster than Hec1-WT (0.9 ± 0.1 μm/min), and moved farther than Hec1-WT (1.0 ± 0.2 versus 0.7 ± 0.1 μm; Figures 1H and 1I; Table 1). These responses led to little overshoot in K-K distance above baseline during dynein pulling (Figure 1G).

Please cite this article in press as: Long et al., Hec1 Tail Phosphorylation Differentially Regulates Mammalian Kinetochore Coupling to Polymerizing and Depolymerizing Microtubules, Current Biology (2017), http://dx.doi.org/10.1016/j.cub.2017.04.058

Table 1. Role of Hec1 Tail Phosphorylation in Regulating the Mechanics of the Mammalian Kinetochore-Microtubule Interface

Measurement	Experimental Condition			t Test[a]
	Hec1-WT	Hec1-9A	Hec1-9D	
Assay: K-Fiber Ablation (Figure 1)				
Number of kinetochores (cells)	13 (4)	17 (8)	10 (7)	
K-K distance before ablation (μm)	2.0 ± 0.1	2.5 ± 0.1	1.4 ± 0.1	WT,9A*; WT,9D*; 9A,9D*
Time at max K-K distance after ablation (s)	95 ± 7	47 ± 5	N/A[b]	WT,9A*
Front kinetochore speed during poleward movement (μm/min)	1.7 ± 0.3	1.6 ± 0.2	1.8 ± 0.2	n.s.
Distance back kinetochore moves during first 30 s of dynein pulling (μm)	0.7 ± 0.1	0.4 ± 0.1	1.0 ± 0.2	WT,9A*; 9A,9D*
Back kinetochore speed during poleward movement (μm/min)	0.9 ± 0.1	0.6 ± 0.1	1.7 ± 0.4	WT,9A*; WT,9D*; 9D,9A*
Assay: Metaphase Spindle Photomarking (Figure 2)				
Number of kinetochores (cells)	57 (29)	60 (24)	27 (8)	
Poleward microtubule flux (μm/min)	0. 65 ± 0.05	0.50 ± 0.03	0.73 ± 0.07	WT,9A*; 9D,9A*
Kinetochore velocity with respect to microtubule lattice (μm/min)	0.76 ± 0.04[c]	0.51 ± 0.03[c]	N/A[c]	WT,9A*
Kinetochore velocity > 0 (toward plus end) with respect to microtubule lattice (μm/min)	1.25 ± 0.03[c]	0.83 ± 0.03[c]	N/A[c]	WT,9A*
Assay: Kinetochore Ablation (Figure 3)				
Number of kinetochores (cells)	17 (14)	21 (12)	18 (13)	
K-K distance before ablation (μm)	2.3 ± 0.1	2.6 ± 0.1	1.7 ± 0.1	WT,9A*; WT,9D*; 9A,9D*
Poleward kinetochore velocity after sister ablation (μm/min)	2.0 ± 0.2	2.1 ± 0.2	2.3 ± 0.2	n.s.
Poleward kinetochore velocity relative to microtubule lattice after sister ablation (μm/min)[d]	1.5 ± 0.2	1.4 ± 0.2	1.6 ± 0.2	n.s.
Time between front sister ablation and back kinetochore switch (s)	5 ± 3	2 ± 2	4 ± 2	n.s.

Data are presented as mean ± SEM. See also Figures 1, 2, and 3. N/A, not applicable; n.s., not significant.

[a]$p < 0.05$ is used as a threshold for statistical significance using two-tailed Student's t test. The abbreviations in the t test column indicate which of the condition pairs are significantly different (e.g., WT,9D* indicates a significant difference between Hec1-WT and Hec1-9D).

[b]There is no meaningful maximum K-K distance after ablation for Hec1-9D due to the variability of traces and lack of overshoot above baseline K-K distance from before ablation.

[c]We made these calculations only on the subset of the data collected using photoactivation (Hec1-WT, n = 42 and Hec1-9A, n = 34 kinetochores) because it allowed longer tracking of oscillations. We did not measure kinetochore velocities in Hec1-9D spindles because we were not able to track photomarks for long enough of the kinetochore oscillation cycle.

[d]To adjust velocities to be relative to the microtubule lattice, we assumed poleward flux was unchanged from metaphase measurements (Figure 2).

Dephosphorylating the Hec1 tail makes the back kinetochore less mobile in response to force: the back kinetochore moves more slowly and a shorter distance and takes longer to recover, despite being under higher forces. Phosphorylating the Hec1 tail has the opposite consequences. Thus, Hec1 tail phosphorylation controls both the magnitude and timescale of the back kinetochore's response to spindle forces, and thereby sets the effective elasticity and viscosity of the spindle's reorganization in response to force. Hec1 phosphorylation regulates the back kinetochore's ability to move when bound to polymerizing microtubules under force. It could do so by directly changing friction on the microtubule lattice, or produce an apparent change in friction by setting the polymerization dynamics at the microtubule tip.

Hec1 Tail Phosphorylation Regulates Friction on Mammalian Kinetochores Bound to Polymerizing Microtubules

To probe the relationship between Hec1 tail phosphorylation and friction, we measured how Hec1 tail phosphorylation changes the velocity—and the friction coefficient, assuming similar forces—between kinetochore and polymerizing microtubules. To determine kinetochore velocity relative to the microtubule lattice, we tracked kinetochores with Hec1-EGFP phosphomutants and concurrently measured k-fiber poleward flux [18] by either photomarking photoactivatable (PA)-GFP-tubulin or photobleaching GFP-tubulin (Figures 2A–2C). K-fiber flux velocities were lower in Hec1-9A (0.50 ± 0.03 μm/min; n = 60) than in Hec1-9D (0.73 ± 0.07 μm/min; n = 27) or WT cells (0.65 ± 0.05 μm/min; n = 57), although spindle length did not change (Figures 2D and 2E; Table 1). Consistent with Hec1 tail phosphorylation decreasing friction, kinetochore velocity with respect to the microtubule lattice during polymerization was higher in Hec1-WT (1.20 ± 0.03 μm/min; n = 720; Movie S4) than in Hec1-9A cells (0.80 ± 0.03 μm/min; n = 940; Movie S4) (Figure 2F; Table 1). Thus, the interface remains dynamic and is never locked within the cell's Hec1 tail phosphorylation range; the kinetochore (as a "slip clutch" [4]) can always slip to reduce force on the chromosome—and prevent detachment from microtubules [19].

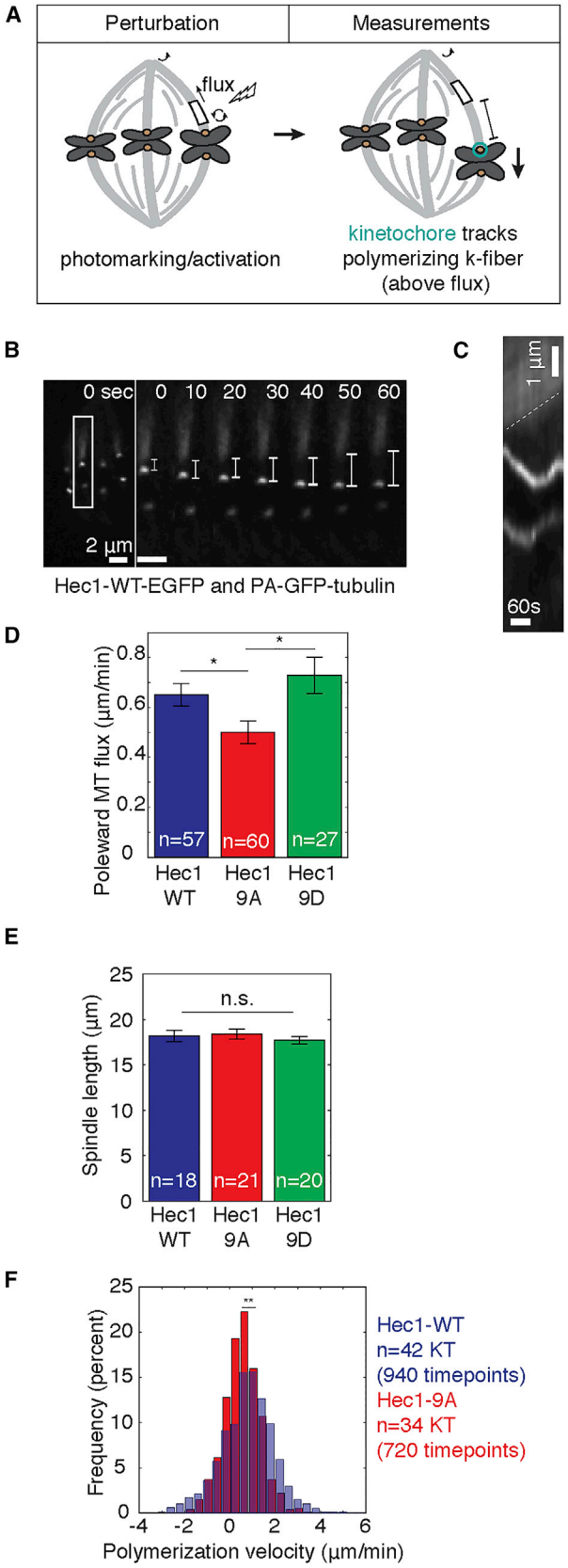

Figure 2. Hec1 Tail Phosphorylation Regulates Friction on Mammalian Kinetochores Bound to Polymerizing Microtubules

(A) Assay to measure kinetochore velocity relative to the microtubule lattice, tracking kinetochores and poleward k-fiber microtubule flux by photomarking.

(B and C) Representative time lapses of Hec1-EGFP and PA-GFP-tubulin PtK2 cells in a Hec1 RNAi background (B) and kymograph of poleward microtubule flux (dotted line) measured by photoactivation (C). Time 0:00 corresponds to photoactivation. The distance between the photomark and the kinetochore (ruler) provides velocity relative to the microtubule lattice.

(D) Microtubule flux rate (mean ± SEM; *p < 0.05, Student's t test) in cells with Hec1-WT, Hec1-9A, or Hec1-9D kinetochores (n, number of k-fibers). MT, microtubule.

(E) Spindle length (mean ± SEM; p = 0.76, one-way ANOVA) in cells with Hec1-WT, Hec1-9A, or Hec1-9D kinetochores (n, number of cells).

(F) Histogram of kinetochore velocity relative to the microtubule lattice (**p < 0.01, Student's t test). Hec1-9D kinetochore oscillations were too variable to quantify (see STAR Methods).

See also Movie S4.

These data are consistent with Hec1 being a component of a frictional interface of kinetochores with microtubules—whose location was inferred to be in the outer kinetochore [20]. Hec1 tail phosphorylation is well suited to tune the effective friction coefficient, and thus the force-velocity relationship, between the mammalian kinetochore and microtubules during polymerization, and to do so in a force range relevant to spindle function.

Hec1 Tail Phosphorylation Does Not Disrupt the Mammalian Kinetochore's Ability to Couple to Depolymerizing Microtubules

Because we found that Hec1 tail phosphorylation decreases kinetochore friction with microtubules during polymerization (Figures 1 and 2), we asked whether it also affects the ability to couple to depolymerizing microtubules. Perturbing Hec1 phosphoregulation changes how metaphase sister kinetochores move [13, 14], but when sister kinetochores are linked (Figures 1 and 2) the coupling to depolymerizing microtubules can never be probed directly, as it is always resisted by its sister. Anaphase kinetochores could provide a solution, but kinetochore biochemistry changes between metaphase and anaphase [21]. Hence, we turned to laser ablation to physically separate sister kinetochores: after ablating one sister, the remaining sister moves toward its pole as its k-fiber depolymerizes [1, 22] (Figures 3A and 3B).

After sister ablation, Hec1-WT kinetochores initially moving poleward speed up, from 1.2 ± 0.2 μm/min (we infer these are depolymerizing microtubules since the velocity is faster than tubulin flux; Figure 2D) to 2.3 ± 0.2 μm/min (n = 10; p < 0.01; Figures 3C and 3D). This acceleration is consistent with the sister, bound to polymerizing microtubules before ablation, providing resistance. In turn, WT kinetochores initially moving away from their pole (polymerizing microtubules) at 0.7 ± 0.1 μm/min switch to poleward movement at 2.1 ± 0.1 μm/min (n = 14; Figures 3C and 3D; Movie S5). The directional switch and kinetochore velocity we measure here are faster than those we measured after k-fiber ablation (Figure 1), which is most likely because here there is no resistance from the sister k-fiber interacting with the spindle. Surprisingly, Hec1-9A (Movie S6) and Hec1-9D (Movie S7) kinetochores, which had perturbed K-K distances (Table 1), moved poleward at the same velocity as Hec1-WT

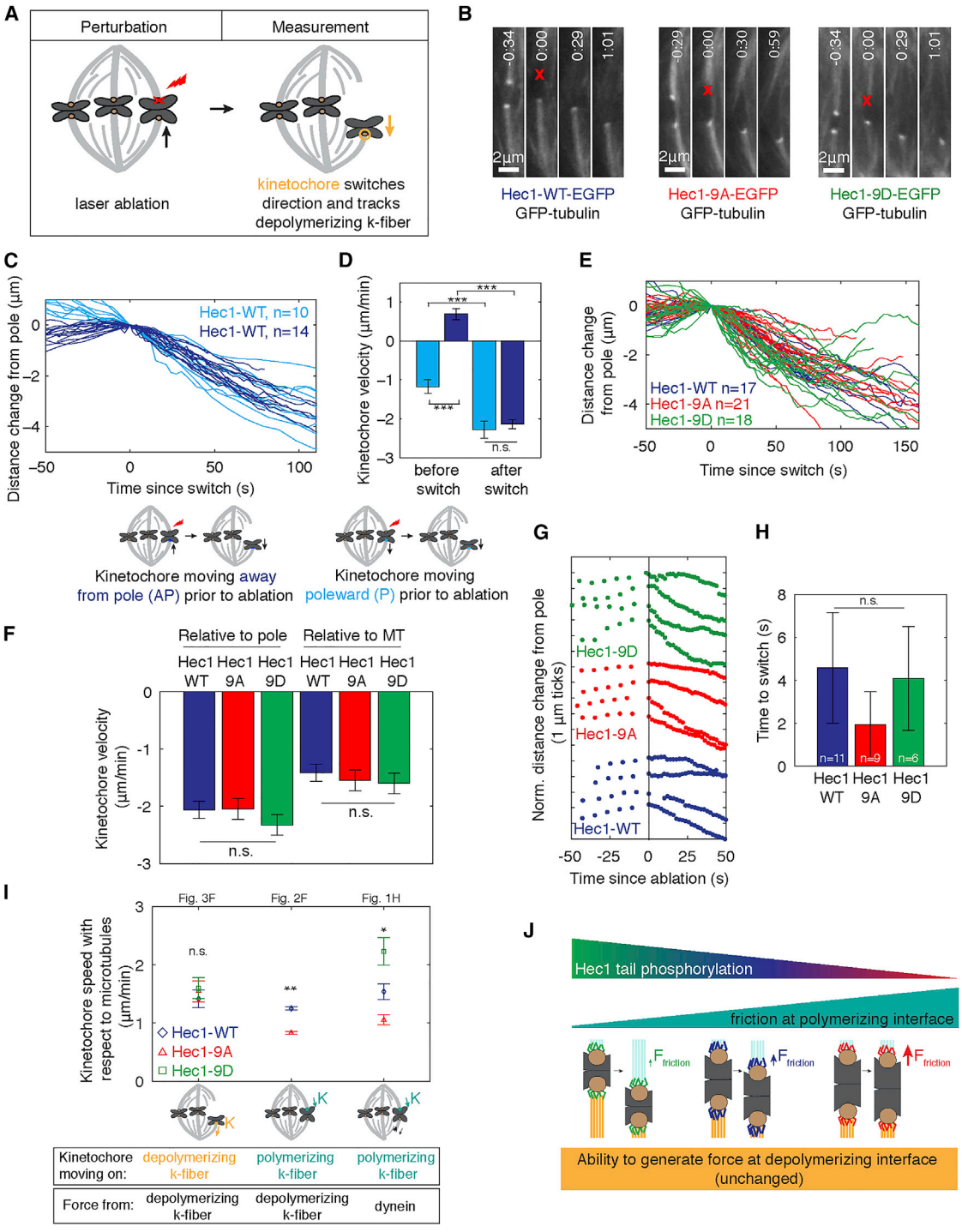

Figure 3. Hec1 Tail Phosphorylation Does Not Disrupt the Mammalian Kinetochore's Ability to Couple to Depolymerizing Microtubules

(A) Assay to decouple sister kinetochores using laser ablation (red X) of one sister kinetochore to probe the remaining sister's ability to track depolymerizing microtubules.

(B) Time lapse of Hec1-WT-EGFP, Hec1-9A-EGP, or Hec1-9D-EGFP and GFP-tubulin in PtK2 cells before and after kinetochore ablation.

(C) Response of kinetochores to sister ablation, colored by pre-ablation direction (n, number of kinetochores).

(D) Kinetochore velocity relative to the pole before and after its direction switch following sister ablation (error bars, mean ± SEM; ***$p < 0.001$, Student's t test).

(E) Responses of kinetochores to sister ablation (n, number of kinetochores).

(F) Kinetochore velocity after switching to poleward motion (depolymerization) due to ablation of the sister. Kinetochore velocities relative to the pole (left) or to the microtubule lattice (right; adjusted for differences in flux from Figure 2) (same dataset as in D, mean ± SEM; ns, not significant; Student's t test).

(G and H) Example traces (G) and mean delay of kinetochores switching direction after sister ablation (H) (error bars, mean ± SEM; Student's t test).

(legend continued on next page)

after sister ablation (2.0 ± 0.2 μm/min, n = 21 and 2.3 ± 0.2 μm/min, n = 18, respectively; Figures 3B, 3E, and 3F; Table 1). As kinetochores approach poles, kinetochore velocity remained unchanged despite chromosomes experiencing higher polar ejection forces [22, 23]. Although more data would be needed to make a stronger statement, we found that, within our ~2 s resolution, the different Hec1 phosphomutants had indistinguishable times to switch directions—suggesting that Hec1 tail phosphorylation may not directly regulate the kinetochore directional switching (Figures 3G and 3H). Thus, although Hec1 tail phosphorylation regulates the kinetochore's ability to couple to polymerizing microtubules (Figures 1 and 2), it does not affect its ability to couple to and track depolymerizing microtubules or its poleward velocity (Figure 3).

DISCUSSION

Accurate chromosome segregation requires the kinetochore to be able to hold on to both polymerizing and depolymerizing microtubules. However, the molecular basis and regulation of kinetochore attachment to polymerizing and depolymerizing k-fibers are not known. In particular, separately probing kinetochore movement in defined polymerization states has been challenging. Elegant in vitro assays [24, 25] overcome these challenges but are not yet tractable for mammalian kinetochores, whereas in vivo microneedle [26, 27] and laser ablation [1, 22, 28] studies have probed kinetochore mechanics in defined states, but not their molecular basis. Here we use a combination of molecular and mechanical perturbations to determine the contribution of Hec1 tail phosphoregulation to mammalian kinetochore movement on polymerizing and depolymerizing microtubules. We find that through Hec1 tail phosphorylation, the kinetochore can independently regulate its ability to move when bound to polymerizing microtubules without losing its ability to couple to depolymerizing microtubules that actively move chromosomes (Figures 3I and 3J). As the needs of mitosis change, regulation of effective kinetochore friction may set how far and how fast chromosomes move in response to force and tune whole-spindle mechanics, for example increasing mechanical coupling across spindle halves as mitosis progresses.

The basis for Hec1's tail regulating kinetochore movement when bound to polymerizing, but not depolymerizing, microtubules is not known. If kinetochore speeds were higher during polymerization than depolymerization states, changes in friction may only be detectable during polymerization; however, we observe higher speeds during depolymerization (Figure 3I; Table 1). Direction-specific regulation could in principle arise from differences in microtubule plus-end tip structure, but this structure so far appears not to differ between sisters [29]. Alternatively, Hec1 structure may vary when bound to polymerizing versus depolymerizing microtubules [30, 31], or proteins other than Hec1 may bear load and govern chromosome velocity during depolymerization [32, 33]. To uncover the molecular basis for Hec1 tail phosphorylation's direction-dependent role, it will be essential to determine whether such phosphorylation regulates friction directly (by changing the tail's microtubule affinity) or indirectly (by changing how its other domains, or other proteins, interact with microtubules), and whether and how it affects k-fiber microtubule dynamics. In order to answer such questions, we will need tools to more tightly control and measure kinetochore composition and corresponding microtubule properties in cells. For example, here we cannot uncouple whether Hec1-9D observations stem from phosphorylation changes only or from residual endogenous Hec1 providing an attachment with fewer microtubules. Better tools would allow us to test whether different microtubule numbers are required for kinetochore coupling to polymerizing and depolymerizing k-fibers. Finally, a future challenge will be to map which proteins contribute to active force generation at the interface with depolymerizing microtubules.

Our work indicates that Hec1 tail phosphorylation regulates the mechanics of the mammalian kinetochore-microtubule interface in a direction-dependent manner, revealing a new level of regulation. Hec1 tail phosphorylation may impact mechanics and regulate microtubule dynamics in both directions in vitro when it is the only coupler [34] but only impact them in polymerization in vivo due to the presence of—and load sharing by—other microtubule-binding proteins in vivo. Consistent with this idea, the Ndc80 tail is nonessential for movement in either direction in budding yeast [35, 36], most likely because both Ndc80 and the Dam1 complexes bind microtubules [37, 38] and provide friction during polymerization, and Dam1 is the main coupler during depolymerization [35]. Functional homologs to Dam1 are being proposed in other eukaryotes [39, 40], and the assay we develop here should be helpful in dissecting the mechanical role of these and other proteins in the active and passive force-generating microtubule interfaces of the mammalian kinetochore. Probing the relative importance of different kinetochore couplers at both interfaces will be critical to understanding the mechanical diversity of kinetochore proteins and functions across systems.

STAR★METHODS

Detailed methods are provided in the online version of this paper and include the following:

- KEY RESOURCES TABLE
- CONTACT FOR REAGENT AND RESOURCE SHARING
- EXPERIMENTAL MODEL AND SUBJECT DETAILS
- METHOD DETAILS
  - Cell culture and transfection of DNA and siRNA
  - Immunofluorescence and immunoblotting
  - Imaging and laser ablation
  - Study design and data inclusion criteria

(I) Summary of the role of Hec1 phosphorylation in regulating kinetochore velocity under different mechanical states. Kinetochore speeds (mean ± SEM) are replotted from the indicated figures (Figure 1H values are adjusted for differences in flux from Figure 2) (*$p < 0.05$, **$p < 0.01$).
(J) Cartoon summarizing the mechanical role of Hec1 tail phosphorylation: it regulates velocity in polymerization (top, cyan) but does not disrupt coupling in depolymerization (bottom, yellow). For simplicity, numbers of microtubules and Hec1 molecules are diagrammed as constant across conditions.
See also Movies S5, S6, and S7.

SUPPLEMENTAL INFORMATION

Supplemental Information includes one figure and seven movies and can be found with this article online at http://dx.doi.org/10.1016/j.cub.2017.04.058.

AUTHOR CONTRIBUTIONS

Conceptualization, A.F.L., D.B.U., and S.D.; Methodology, A.F.L., D.B.U., and S.D.; Investigation, A.F.L. and D.B.U.; Data Curation, A.F.L.; Writing – Original Draft, A.F.L. and S.D.; Writing – Review & Editing, A.F.L., D.B.U., and S.D.; Visualization, A.F.L.; Funding Acquisition, S.D.

ACKNOWLEDGMENTS

We thank Jennifer DeLuca for Hec1-EGFP mutant constructs and advice, Ekaterina Grishchuk, Ted Salmon, Ronald Vale, David Morgan, and David Agard for discussions, and members of the Dumont laboratory for discussions and critical reading of the manuscript. This work was funded by NIH DP2GM119177, NSF CAREER 1554139, the Rita Allen Foundation and Searle Scholars' Program (S.D.), and a NSF Graduate Research Fellowship (A.F.L.).

Received: November 22, 2016
Revised: March 22, 2017
Accepted: April 27, 2017
Published: May 25, 2017

REFERENCES

1. Khodjakov, A., and Rieder, C.L. (1996). Kinetochores moving away from their associated pole do not exert a significant pushing force on the chromosome. J. Cell Biol. *135*, 315–327.
2. Wan, X., Cimini, D., Cameron, L.A., and Salmon, E.D. (2012). The coupling between sister kinetochore directional instability and oscillations in centromere stretch in metaphase PtK1 cells. Mol. Biol. Cell *23*, 1035–1046.
3. Hill, T.L. (1985). Theoretical problems related to the attachment of microtubules to kinetochores. Proc. Natl. Acad. Sci. USA *82*, 4404–4408.
4. Maddox, P., Straight, A., Coughlin, P., Mitchison, T.J., and Salmon, E.D. (2003). Direct observation of microtubule dynamics at kinetochores in *Xenopus* extract spindles: implications for spindle mechanics. J. Cell Biol. *162*, 377–382.
5. Cheeseman, I.M., and Desai, A. (2008). Molecular architecture of the kinetochore-microtubule interface. Nat. Rev. Mol. Cell Biol. *9*, 33–46.
6. Rago, F., and Cheeseman, I.M. (2013). The functions and consequences of force at kinetochores. J. Cell Biol. *200*, 557–565.
7. Sarangapani, K.K., and Asbury, C.L. (2014). Catch and release: how do kinetochores hook the right microtubules during mitosis? Trends Genet. *30*, 150–159.
8. DeLuca, J.G., Gall, W.E., Ciferri, C., Cimini, D., Musacchio, A., and Salmon, E.D. (2006). Kinetochore microtubule dynamics and attachment stability are regulated by Hec1. Cell *127*, 969–982.
9. Cheeseman, I.M., Chappie, J.S., Wilson-Kubalek, E.M., and Desai, A. (2006). The conserved KMN network constitutes the core microtubule-binding site of the kinetochore. Cell *127*, 983–997.
10. Ciferri, C., Pasqualato, S., Screpanti, E., Varetti, G., Santaguida, S., Dos Reis, G., Maiolica, A., Polka, J., De Luca, J.G., De Wulf, P., et al. (2008). Implications for kinetochore-microtubule attachment from the structure of an engineered Ndc80 complex. Cell *133*, 427–439.
11. Guimaraes, G.J., Dong, Y., McEwen, B.F., and DeLuca, J.G. (2008). Kinetochore-microtubule attachment relies on the disordered N-terminal tail domain of Hec1. Curr. Biol. *18*, 1778–1784.
12. Powers, A.F., Franck, A.D., Gestaut, D.R., Cooper, J., Gracyzk, B., Wei, R.R., Wordeman, L., Davis, T.N., and Asbury, C.L. (2009). The Ndc80 kinetochore complex forms load-bearing attachments to dynamic microtubule tips via biased diffusion. Cell *136*, 865–875.
13. DeLuca, K.F., Lens, S.M.A., and DeLuca, J.G. (2011). Temporal changes in Hec1 phosphorylation control kinetochore-microtubule attachment stability during mitosis. J. Cell Sci. *124*, 622–634.
14. Zaytsev, A.V., Sundin, L.J.R., DeLuca, K.F., Grishchuk, E.L., and DeLuca, J.G. (2014). Accurate phosphoregulation of kinetochore-microtubule affinity requires unconstrained molecular interactions. J. Cell Biol. *206*, 45–59.
15. Zaytsev, A.V., Mick, J.E., Maslennikov, E., Nikashin, B., DeLuca, J.G., and Grishchuk, E.L. (2015). Multisite phosphorylation of the NDC80 complex gradually tunes its microtubule-binding affinity. Mol. Biol. Cell *26*, 1829–1844.
16. Elting, M.W., Hueschen, C.L., Udy, D.B., and Dumont, S. (2014). Force on spindle microtubule minus ends moves chromosomes. J. Cell Biol. *206*, 245–256.
17. Sikirzhytski, V., Magidson, V., Steinman, J.B., He, J., Le Berre, M., Tikhonenko, I., Ault, J.G., McEwen, B.F., Chen, J.K., Sui, H., et al. (2014). Direct kinetochore-spindle pole connections are not required for chromosome segregation. J. Cell Biol. *206*, 231–243.
18. Mitchison, T.J. (1989). Polewards microtubule flux in the mitotic spindle: evidence from photoactivation of fluorescence. J. Cell Biol. *109*, 637–652.
19. Matos, I., Pereira, A.J., Lince-Faria, M., Cameron, L.A., Salmon, E.D., and Maiato, H. (2009). Synchronizing chromosome segregation by flux-dependent force equalization at kinetochores. J. Cell Biol. *186*, 11–26.
20. Dumont, S., Salmon, E.D., and Mitchison, T.J. (2012). Deformations within moving kinetochores reveal different sites of active and passive force generation. Science *337*, 355–358.
21. Su, K.-C., Barry, Z., Schweizer, N., Maiato, H., Bathe, M., and Cheeseman, I.M. (2016). A regulatory switch alters chromosome motions at the metaphase-to-anaphase transition. Cell Rep. *17*, 1728–1738.
22. Skibbens, R.V., Rieder, C.L., and Salmon, E.D. (1995). Kinetochore motility after severing between sister centromeres using laser microsurgery: evidence that kinetochore directional instability and position is regulated by tension. J. Cell Sci. *108*, 2537–2548.
23. Ke, K., Cheng, J., and Hunt, A.J. (2009). The distribution of polar ejection forces determines the amplitude of chromosome directional instability. Curr. Biol. *19*, 807–815.
24. Akiyoshi, B., Sarangapani, K.K., Powers, A.F., Nelson, C.R., Reichow, S.L., Arellano-Santoyo, H., Gonen, T., Ranish, J.A., Asbury, C.L., and Biggins, S. (2010). Tension directly stabilizes reconstituted kinetochore-microtubule attachments. Nature *468*, 576–579.
25. Miller, M.P., Asbury, C.L., and Biggins, S. (2016). A TOG protein confers tension sensitivity to kinetochore-microtubule attachments. Cell *165*, 1428–1439.
26. Nicklas, R.B., and Staehly, C.A. (1967). Chromosome micromanipulation. I. The mechanics of chromosome attachment to the spindle. Chromosoma *21*, 1–16.
27. Skibbens, R.V., and Salmon, E.D. (1997). Micromanipulation of chromosomes in mitotic vertebrate tissue cells: tension controls the state of kinetochore movement. Exp. Cell Res. *235*, 314–324.
28. McNeill, P.A., and Berns, M.W. (1981). Chromosome behavior after laser microirradiation of a single kinetochore in mitotic PtK2 cells. J. Cell Biol. *88*, 543–553.
29. McIntosh, J.R., Grishchuk, E.L., Morphew, M.K., Efremov, A.K., Zhudenkov, K., Volkov, V.A., Cheeseman, I.M., Desai, A., Mastronarde, D.N., and Ataullakhanov, F.I. (2008). Fibrils connect microtubule tips with kinetochores: a mechanism to couple tubulin dynamics to chromosome motion. Cell *135*, 322–333.

30. Wang, H.-W., Long, S., Ciferri, C., Westermann, S., Drubin, D., Barnes, G., and Nogales, E. (2008). Architecture and flexibility of the yeast Ndc80 kinetochore complex. J. Mol. Biol. *383*, 894–903.

31. Kudalkar, E.M., Scarborough, E.A., Umbreit, N.T., Zelter, A., Gestaut, D.R., Riffle, M., Johnson, R.S., MacCoss, M.J., Asbury, C.L., and Davis, T.N. (2015). Regulation of outer kinetochore Ndc80 complex-based microtubule attachments by the central kinetochore Mis12/MIND complex. Proc. Natl. Acad. Sci. USA *112*, E5583–E5589.

32. Nicklas, R.B. (1983). Measurements of the force produced by the mitotic spindle in anaphase. J. Cell Biol. *97*, 542–548.

33. Inoué, S., and Salmon, E.D. (1995). Force generation by microtubule assembly/disassembly in mitosis and related movements. Mol. Biol. Cell *6*, 1619–1640.

34. Umbreit, N.T., Gestaut, D.R., Tien, J.F., Vollmar, B.S., Gonen, T., Asbury, C.L., and Davis, T.N. (2012). The Ndc80 kinetochore complex directly modulates microtubule dynamics. Proc. Natl. Acad. Sci. USA *109*, 16113–16118.

35. Suzuki, A., Badger, B.L., Haase, J., Ohashi, T., Erickson, H.P., Salmon, E.D., and Bloom, K. (2016). How the kinetochore couples microtubule force and centromere stretch to move chromosomes. Nat. Cell Biol. *18*, 382–392.

36. Sarangapani, K.K., Akiyoshi, B., Duggan, N.M., Biggins, S., and Asbury, C.L. (2013). Phosphoregulation promotes release of kinetochores from dynamic microtubules via multiple mechanisms. Proc. Natl. Acad. Sci. USA *110*, 7282–7287.

37. Lampert, F., Hornung, P., and Westermann, S. (2010). The Dam1 complex confers microtubule plus end-tracking activity to the Ndc80 kinetochore complex. J. Cell Biol. *189*, 641–649.

38. Tien, J.F., Umbreit, N.T., Gestaut, D.R., Franck, A.D., Cooper, J., Wordeman, L., Gonen, T., Asbury, C.L., and Davis, T.N. (2010). Cooperation of the Dam1 and Ndc80 kinetochore complexes enhances microtubule coupling and is regulated by aurora B. J. Cell Biol. *189*, 713–723.

39. Schmidt, J.C., Arthanari, H., Boeszoermenyi, A., Dashkevich, N.M., Wilson-Kubalek, E.M., Monnier, N., Markus, M., Oberer, M., Milligan, R.A., Bathe, M., et al. (2012). The kinetochore-bound Ska1 complex tracks depolymerizing microtubules and binds to curved protofilaments. Dev. Cell *23*, 968–980.

40. Hanisch, A., Silljé, H.H.W., and Nigg, E.A. (2006). Timely anaphase onset requires a novel spindle and kinetochore complex comprising Ska1 and Ska2. EMBO J. *25*, 5504–5515.

41. Udy, D.B., Voorhies, M., Chan, P.P., Lowe, T.M., and Dumont, S. (2015). Draft de novo transcriptome of the rat kangaroo *Potorous tridactylus* as a tool for cell biology. PLoS ONE *10*, e0134738.

STAR★METHODS

KEY RESOURCES TABLE

REAGENT or RESOURCE	SOURCE	IDENTIFIER
Antibodies		
Mouse anti-Hec1 (Hec1-9G3)	Novus	Cat#NB100-338; RRID: AB_10000917
Human anti-centromere (CREST)	Antibodies, Inc.	Cat#15-234-0001; RRID: N/A
Rat anti-tubulin	AbD Serotec	Cat#MCA77G; RRID: AB_325003
Mouse anti-tubulin (DM1α)	Sigma	Cat#T6199; RRID: AB_477583
Goat anti-mouse IgG-HRP	Santa Cruz Biotechnology	Cat#SC-2055; RRID: AB_631738
Alexa 594 Goat anti-human IgG	Invitrogen	Cat#A11014; RRID: AB_2534081
Alexa 488 Goat anti-mouse IgG (highly cross absorbed)	Invitrogen	Cat# A11001; RRID: AB_2534069
Alexa 647 Goat anti-rat IgG (highly cross absorbed)	Invitrogen	Cat#A21247; RRID: AB_141778
Chemicals, Peptides, and Recombinant Proteins		
SiR-tubulin dye	Spirochrome	Cat#SC-002
Verapamil	Sigma-Aldrich	Cat#V4629
FuGene 6	Roche	Cat#E2691
Viafect	Promega	Cat#E4981
Oligofectamine	Invitrogen/Life Technologies	Cat#12252011
Hoechst 33342	Sigma-Aldrich	Cat#H3570
SuperSignal West Pico Substrate	Thermo Scientific	Cat#34080
Experimental Models: Cell Lines		
PtK2 cells	T. Mitchison	ATCC Cat#CCL-56; RRID: CVCL_0514
Oligonucleotides		
siRNA against PtK Hec1: 5′-AATGAGCCGAATCGTCTAATA-3′	[11]	N/A
Recombinant DNA		
plasmid: WT-Hec1-EGFP	J. DeLuca [8]	N/A
plasmid: 9A-Hec1-EGFP	J. DeLuca [13]	N/A
plasmid: 9D-Hec1-EGFP	J. DeLuca [14]	N/A
plasmid: pEGFP-tubulin	Clonetech	Discontinued (similar to Cat#632488)
plasmid: PA-GFP-tubulin	A. Khodjakov	N/A
Software and Algorithms		
MATLAB (R2013B)	MathWorks	RRID: SCR_001622
StatPlus	AnalystSoft	RRID: SCR_014635
Fiji	ImageJ	RRID: SCR_002285
Other		
35mm MatTek Dishes (poly-D-lysine coated)	MatTek Corporation	Cat#P35GC-1.5-20-C

CONTACT FOR REAGENT AND RESOURCE SHARING

Further information and requests for resources and reagents should be directed to and will be fulfilled by the Lead Contact, Sophie Dumont (sophie.dumont@ucsf.edu).

EXPERIMENTAL MODEL AND SUBJECT DETAILS

PtK2 cells (gift from T. Mitchison, Harvard University) were cultured in MEM (Invitrogen) supplemented with sodium pyruvate (Invitrogen), nonessential amino acids (Invitrogen), penicillin/streptomycin, and 10% qualified and heat-inactivated fetal bovine serum (FBS) (Invitrogen) and maintained at 37°C and 5% CO_2. PtK2 cells are male kidney epithelial cells from the rat kangaroo (*Potorous tridactylus*). The PtK2 cells used in this study were not authenticated, but we sequenced their transcriptome [41] and it was consistent with our overall expectation from related marsupials.

METHOD DETAILS

Cell culture and transfection of DNA and siRNA

For imaging, PtK2 cells were imaged in phenol red free MEM (Invitrogen) supplemented with antibiotics and serum as for cell culture. PtK2 cells were transfected with WT-Hec1-EGFP, 9A-Hec1-EGFP, or 9D-Hec1-EGFP (human Hec1 phosphomutants in pEGFP-N1 vector; gifts from J. DeLuca, Colorado State University, CO) [8, 13, 14] or pEGFP-tubulin (Clonetech) or PA-GFP-tubulin (gift A. Khodjakov, Wadsworth Center, Albany, NY). siRNAs directed to PtK Hec1 (5′-AATGAGCCGAATCGTCTAATA-3′) were purchased from Invitrogen or Sigma-Aldrich, and do not target human Hec1 [11]. For knock down and rescue experiments, cells were transfected with DNA using 4 μL FuGENE6 (Roche) or 6 μL ViaFect (Promega) and 0.5-1 μg plasmid DNA after a 20 min incubation. After incubation, the DNA solution was added to trypsinized cells in solution and mixed gently before plating at 40%–60% confluency on #1.5 25 mm coverslips (acid cleaned and poly-L-lysine coated) for immunofluorescence experiments or 35 mm glass-bottom dishes (poly-D-lysine coated; MatTek Corporation) for live imaging. After 24 hr, cells previously transfected with plasmid DNA were transfected with 8 μL 20 μM siRNA against PtK Hec1 and 4 μl Oligofectamine in OptiMem after a 20 min incubation and then supplemented with 1ml OptiMEM with 10% FBS. Cells were assayed 48 hr after siRNA transfection. Control cells with Hec1 siRNA (and no rescue construct) robustly displayed phenotypes consistent with Hec1 knockdown (Figure S1). In Figure 1, 6/10 of the Hec1-9D-EGFP cells included tubulin labeled with 100 nM SiR-tubulin dye (Spirochrome) and 10 μM verapamil (Sigma-Aldrich) after incubation for 1h.

Immunofluorescence and immunoblotting

To validate knockdown (Figure S1), mock control and siHec1 treated cells were fixed 48 hr after siRNA transfection in 95% methanol with 5 mM EGTA for 3 min. The following antibodies and dyes were used: mouse Hec1-9G3 (1:1000, Novus), human anti-centromere protein (CREST,1:25, Antibodies, Inc.), rat anti-tubulin (1:500, AbD Serotec), Alexa 594 goat anti-human IgG (1:500, Invitrogen), Alexa 488 goat anti-mouse IgG highly cross adsorbed (1:500, Invitrogen), Alexa 647 goat anti-rat IgG highly cross absorbed (1:500, Invitrogen), and Hoechst 33342 (1:1000, Sigma-Aldrich). For immunoblotting to validate knockdown, PtK2 cells were lysed 48 hr after siRNA transfection. The following antibodies and dyes were used: mouse anti-tubulin DM1α (1:5,000, Sigma) and mouse anti-Hec1 9G3 (1:1,000, Novus), goat anti-mouse IgG-HRP (1:10,000, Santa Cruz Biotechnology). Blots were exposed with SuperSignal West Pico Substrate (Thermo Scientific) and imaged with a Bio-Rad ChemiDoc XRS+ system.

Imaging and laser ablation

Live cells were imaged using an inverted microscope (Eclipse Ti-E; Nikon) with a spinning disk confocal (CSU-X1; Yokogawa Electric Corporation), head dichroic Semrock Di01-T405/488/568/647 for multicolor imaging or Di01-T488 for GFP only imaging, equipped with 405 nm (100 mW), 488 nm (120mW), 561 nm (150mW), and 642 nm (100mW) diode lasers, emission filters ET455/50M, ET525/50M, ET630/75M and ET690/50M for multicolor imaging and ET500LP (Chroma Technology) for GFP imaging, and an iXon3 camera (Andor Technology) operated by MetaMorph (7.7.8.0; Molecular Devices) [16]. Cells were imaged with phase contrast (200-400ms exposure) and 488nm laser light (75-100ms exposure) through a 100x 1.45 Ph3 oil objective and 1.5x lens every 2-10 s, in a stage-top incubation chamber (Tokai Hit) maintained at 30°C and 5% CO_2. Laser ablation (30-40 3-ns pulses at 20Hz) with 514 or 551nm light was performed using the MicroPoint Laser System (Photonic Instruments) [16]. For laser ablation experiments, images were acquired more slowly prior to ablation and then acquired more rapidly after ablation (typically 8 s prior and 4 s after ablation, except the latter was 2 s for Figure 3G). Successful k-fiber ablation was verified by loss of tension across the centromere (Figure 1). Successful kinetochore ablation was verified by change in movement of the remaining sister kinetochore and depolymerization of the k-fiber associated with the ablated kinetochore (Figure 3). Photomarking was performed using the MicroPoint to deliver several pulses of either 514nm light to bleach GFP-tubulin (acquiring every 2-3 s for at least 30 s) or 405nm light to activate PA-GFP-tubulin (acquiring every 10 s for at least 60 s) (Figures 2B and 2C). Fixed cells (Figure S1 only) were imaged with exposure times of 5-200ms with DAPI, GFP, TRITC, and CY5 filter cubes and a mercury arc lamp on a Zeiss AxioPlan2 epifluorescence microscope (operated by MicroManager 1.4.13) with a 100x 1.4 DIC oil objective and a QIClick camera (QImaging).

Study design and data inclusion criteria

The criteria for inclusion of cells in our study were that they must exhibit GFP expression and phenotype consistent with successful introduction of the relevant Hec1 WT or mutant construct as well as exhibit responses consistent with technically successful ablation (as described in the above section). Successful transfection and expression of Hec1 constructs was assessed by visualizing EGFP at kinetochores and, for mutants, by confirming that each cell examined had the expected K-K distance change. Cells expressing Hec1-9D-EGFP in a Hec1 RNAi background had widely varied spindle architecture and we included in our analysis cells that had visible EGFP expression and low K-K distance indicative of rescue but that still were able to form metaphase spindles and oscillate – which may include cells that still have a residual amount of endogenous Hec1 remaining.

We did not pre-estimate a required sample size before performing experiments nor did we blind or randomize samples during experimentation or analysis since the mutant phenotypes are readily apparent by eye. The experiments in this study are low throughput, which does not enable us to report averages from multiple independent replicate experiments and instead we pool cells from across different independent experiments.

QUANTIFICATION AND STATISTICAL ANALYSIS

Tracking and quantification of spindle features

Kinetochores, photomarks, ablation sites, and spindle poles were manually tracked from overlaid phase-contrast time-lapse and Hec1-EGFP (sometimes with GFP-tubulin or PA-GFP-tubulin) movies using a home-written MATLAB (R2013b Version 8.2) program. Spindle poles were identified using the center of the GFP tubulin enriched region at the ends of the spindle. When no tubulin was co-transfected (Figure 1), approximate spindle pole position was determined using phase contrast images (where the spindle can be identified since it excludes mitochondria). We manually selected the inflection points in kinetochore position as the start and end points of movement in one direction using plots of kinetochore position relative to the pole over time. We then calculated kinetochore velocity by fitting to a linear function (Figures 1H, 1I, 3D, and 3F; Table 1). We report (Figure 1I) the distance traveled by kinetochores during the first 30 s after the start of dynein-induced poleward motion of a kinetochore pair, to avoid variability coming from differences in the duration of the poleward transport response. Poleward microtubule flux (Figure 2D) was calculated by measuring the position of the edge of the photomark closest to the kinetochore over time relative to the initial position (for PA-GFP-tubulin) for at least ~60 s, or by measuring the position of the bleach mark over time relative to the pole (for GFP-tubulin) for as long as possible and in both cases performing a linear regression. Kinetochore velocity with respect to the microtubule lattice (k-fiber polymerization velocity) was calculated by measuring the distance between kinetochore and photomark on the same k-fiber for each pair of time points to get an instantaneous velocity that were pooled from different cells (Figure 2E). Kinetochore velocities relative to the microtubule lattice after ablation were calculated by subtracting the mean value of poleward microtubule flux (Figure 2B) from the measured velocity (Figures 3F and 3I; Table 1). Time to kinetochore switching after ablation (Figure 3H) was measured from the first frame after ablation to the frame when the kinetochore switched direction.

Movie preparation

Movies were formatted for publication using Fiji (Version 2.0.0-rc-43/1.51h) and set to play at 60x relative to real time. Movies were corrected to play at a constant frame rate, even when the acquisition rate was not constant.

Statistical analysis

Data are reported as mean ± SEM and for average traces (Figure 1) data were collected into 8 s wide bins before averaging. One-way ANOVA were performed using StatPlus (Version v6; AnalystSoft) to compare between more than two experimental conditions and followed up with two-tailed unpaired Student's t tests performed using MATLAB, without testing for whether assumptions for normality were met due to low sample sizes. We used $p < 0.05$ as the threshold for statistical significance and indicated in the figure and figure legend if the p value was lower than 0.05, 0.01 or 0.001 using asterisks (* or ** or ***, respectively). 'n' always refers to number of kinetochores or kinetochore-fibers except in Figure 2E where 'n' refers to number of cells and Figure 2F where 'n' refers to the number of time points pooled across kinetochores in each experimental condition. Both the number of kinetochores and the number of cells are provided in Table 1 for clarity, but statistical tests were always performed on kinetochore measurements pooled from different cells collected across at least two independent experiments. Sample sizes, statistical tests and p values are also indicated in the text, figures and figure legends where relevant.